GEOCHEMISTRY

Nitrogen isotope ratios trace high-pH conditions in a terrestrial Mars analog site

Eva E. Stüeken[1,2*†], Christopher Tino[3*], Gernot Arp[4], Dietmar Jung[5], Timothy W. Lyons[2,3]

High-pH alkaline lakes are among the most productive ecosystems on Earth and prime targets in the search for life on Mars; however, a robust proxy for such settings does not yet exist. Nitrogen isotope fractionation resulting from NH_3 volatilization at high pH has the potential to fill this gap. To validate this idea, we analyzed samples from the Nördlinger Ries, a Miocene impact crater lake that displayed pH values up to 9.8 as inferred from mineralogy and aqueous modeling. Our data show a peak in $\delta^{15}N$ of +17‰ in the most alkaline facies, followed by a gradual decline to around +5‰, concurrent with the proposed decline in pH, highlighting the utility of nitrogen isotopes as a proxy for high-pH conditions. In combination with independent mineralogical indicators for high alkalinity, nitrogen isotopes can provide much-needed quantitative constraints on ancient atmospheric P_{CO_2} (partial pressure of CO_2) and thus climatic controls on early Earth and Mars.

INTRODUCTION

Jezero crater, the designated landing site for the Mars 2020 rover, has smectite clays and carbonate sequences that imply circumneutral-to-alkaline aqueous conditions during the earliest portions of the crater's lacustrine history (*1*, *2*). However, while mineral associations mirror a combination of salinities, temperatures, redox, and pH [e.g., (*3*)], a specific approximation of ancient pH conditions is not possible on this basis. Developing a method for distinguishing between circumneutral and high-pH environments is astrobiologically notable because high-pH alkaline lakes are the most bioproductive natural aquatic systems on Earth, and their productivity is almost exclusively driven by Bacteria and Archaea (*4*). The Miocene Ries crater lake in southern Germany (Fig. 1) is an ideal testbed for testing and calibrating such proxies.

The Nördlinger Ries is widely recognized as an analog for Martian craters and specifically related ejecta fluidization, post-impact hydrothermal activity, and aqueous sedimentation on early Mars [e.g., (*5*–*8*)]. The Ries crater formed about 14.8 million years ago through an asteroid impact that excavated 500 to 650 m of Triassic-Jurassic and Tertiary sedimentary rocks and more than 2 km of the underlying Variscan crystalline basement. The resulting transient cavity collapsed quickly, leaving behind a 600-m-deep and 26-km-wide depression that filled with water and sediments over time (*9*) and hosted diverse biological assemblages throughout its approximately 0.3- to 2-million-year history (*8*, *10*). Partial melting of target rocks enhanced physical and chemical weathering with significant effects on sediment composition (*11*) and lake water chemical evolution (*7*)—differing from standard terrestrial lake basins but potentially analogous to Martian basins.

Specifically, the mineralogy of the sediments deposited within the crater on top of the crater suevite (a melt-bearing, polymict impact breccia) indicates that weathering of crystalline rock–derived lithic breccias and glassy melt fragments had a substantial effect on the chemistry of the lake waters (*8*). In particular, the abundance of the zeolite minerals analcime and clinoptilolite in the laminite member of the lower sediment package and the near absence of diatom tests in this interval (Fig. 2), paired with covarying carbon and oxygen isotopes, have been taken as evidence for high alkalinity that resulted from silicate weathering and strongly evaporative conditions in a closed-basin lake (*8*, *10*, *12*). Zeolites have also been detected on Mars where they are thought to have formed during aqueous alteration of volcanic glass (*13*). Aqueous geochemical modeling of the Ries lake suggests a pH of up to 9.8 during this zeolite-rich interval (*8*). The lake likely became progressively more saline over time, as the pH decreased when inflowing waters became chemically controlled by weathering of the Bunte Breccia and Jurassic sedimentary rocks (*8*). This model would have important implications for our understanding of habitats in Martian crater lakes. First, it is likely that weathering of suevite-like deposits on Mars, including impact and volcanic breccia, would result in high-pH waters in many fresh impact settings. This effect would likely be enhanced on Mars because the crust is relatively more mafic, and glasses of mafic composition have been shown to elevate the pH more strongly than silica-rich glasses [cf. (*14*, *15*)]. Second, significant shifts in pH due to chemical lake evolution can be expected in terranes with layered composition, i.e., where rapidly weathering ash and melt fragments initially create high-pH conditions before weathering of more crystalline basement rocks shifts the pH toward neutral values, similar to the Ries crater. Although basaltic rocks prevail in many Martian regions at the surface, including Jezero crater, there is increasing indication of a more diverse lithologic crust composition including felsic magmatic rocks (*16*). This observation also applies to Gale crater, which hosted a permanent, potentially habitable lake (*17*). It is therefore important to develop a geochemical proxy that is sensitive to high-pH conditions in the sedimentary record of Mars as well as the early Earth, where relatively unstable proxies such as zeolites and biomarkers may not be preserved. The relevance of these conditions is elevated by their strong impacts on life.

Boron isotopes are commonly used as a pH proxy in the marine realm, but this technique requires knowledge of the boron isotopic composition of the water column. Other proxies, such as rare earth elements or calcium isotopes, also require additional parameters,

[1]School of Earth and Environmental Sciences, University of St. Andrews, St. Andrews, Fife, KY16 9AL Scotland, UK. [2]Virtual Planetary Laboratory, University of Washington, Seattle, WA 98195, USA. [3]Department of Earth Sciences, University of California, Riverside, CA 92521, USA. [4]Georg-August-Universität Göttingen, Geowissenschaftliches Zentrum, Goldschmidtstrasse 3, 37077 Göttingen, Germany. [5]Bayerisches Landesamt für Umwelt, Geologischer Dienst, Hans-Högn-Straße 12, 95030 Hof/Saale, Germany.
*These authors contributed equally to this work.
†Corresponding author. Email: ees4@st-andrews.ac.uk

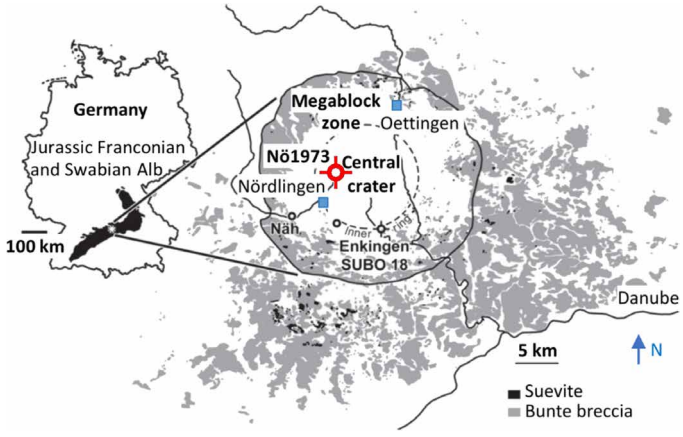

Fig. 1. Map showing the location of the Ries crater and the Nördlingen 1973 drill hole. Adapted from Arp *et al.* (*8*).

such as source rock composition or alkalinity. In this study, we tested nitrogen isotopes as an alternative approach. During diagenesis, degrading biomass releases NH_4^+, which partitions into NH_3 with a pK_a (where K_a is the acid dissociation constant) of 9.2 at standard pressure and temperature. NH_3 is volatile and can escape into the atmosphere, as is observed in modern alkaline lakes during water column overturn (*18*). This process imparts a large isotopic fractionation ($\varepsilon \approx \delta_{product} - \delta_{reactant}$) of −42‰ in $\delta^{15}N$ (= $[(^{15}N/^{14}N)_{sample}/(^{15}N/^{14}N)_{air} - 1] \times 1000$), rendering the residual NH_4^+ isotopically heavy (*19*). The fractionation decreases with temperature, but it is still as high as −33‰ at 70°C. High $\delta^{15}N$ values >10‰ in sediments from evaporitic lakes have therefore been used as indicators of elevated pH during the time of deposition (*20*–*23*). However, it is so far unknown whether such large isotopic fractionation can also be produced by redox processes (e.g., denitrification) in stratified saline lakes under circumneutral pH. The chemical trends inferred from the Ries crater (Fig. 2) (*8*) can thus serve as an ideal natural laboratory to explore the utility of $\delta^{15}N$ in consolidating a multitude of geochemical measurements into single, reliable proxy for high-pH conditions.

Sampling

We collected samples from the Nördlingen 1973 drill core (Fig. 2), which was drilled in the central crater and intersects most of the lacustrine sedimentary infill. The basal member, which sits directly on top of the suevite, is composed of sandstones and conglomerates of reworked suevite and basement rocks that may have been deposited in debris flows (*10*). This unit transitions into a laminated marl with bituminous shale intercalations (laminite member), representing a stratified permanent lake. The laminite member is followed by a greenish-gray poorly stratified marlstone (marl member), which has been interpreted as evidence of shallowing (*10*). The marlstone is capped by a gray claystone with thin allochthonous coal seams as well as gypsum pseudomorphs that likely represent highly fluctuating water depths and salinities (*24*). We selected samples from the top of the basal member to the middle of the clay member with a resolution of a few meters (Table 1).

RESULTS

At the base of the laminite member, $\delta^{15}N$ shows a sharp increase over an interval of about 15 m from values around +3‰ to a maximum of +17‰ (Table 1 and Fig. 2). The values then decrease gradually toward +5‰ at the top of the core. The interval with the highest values (>+10‰) in the bituminous laminite member also contains a greater abundance of zeolites and much lower abundances of macrofossils (Fig. 2) (*10*). The total nitrogen (TN) content broadly covaries with total organic carbon (TOC, Fig. 3A), indicating that most of the nitrogen is derived from buried organic matter. This relationship does not preclude the presence of clay-bound ammonium, which inevitably forms during diagenesis (*25*) and may explain some of the deviations in the TN-TOC cross-plot, but this process does not impart a significant isotopic fractionation [<2‰, (*26*)]. Horizons with unusually high TOC correspond to bitumen enrichments in the laminite member and thin coal beds in the clay member. $\delta^{15}N$ does not covary with C/N ratios (Fig. 3C), indicating that $\delta^{15}N$ values have not suffered from metamorphic alteration (*27*), which is consistent with post-depositional geothermal heating to a maximum of 60°C as inferred from vitrinite reflectance (*28*). The slight covariance between $\delta^{15}N$ and TN (Fig. 3B) is most likely a primary feature linked to environmental conditions that raised $\delta^{15}N$ while favoring biomass preservation under anoxic conditions, as indicated by concurrently high TOC (Fig. 3A). $\delta^{13}C_{org}$ initially increases gradually up-section in the laminite member from about −27 to −20‰ before dropping back to a more constant value of around −26‰ in the overlying strata. This trend broadly agrees with previous measurements of $\delta^{13}C_{carb}$ (Fig. 2) (*12*), suggesting that primary producers are tracking the composition of dissolved CO_2, which likely becomes isotopically heavier as a result of evaporation (*29*).

DISCUSSION

Nitrogen isotopes can be fractionated by several biogeochemical processes. The major source of nitrogen to surface environments is biological N_2 fixation with a small fractionation of −4 to 0‰ [reviewed in (*30*)]. The most important mechanisms with fractionations of more than 10‰ include nitrification of NH_4^+ to NO_3^- ($\varepsilon \approx -1$ to −25‰), reduction of NO_3^- to N_2 (denitrification, $\varepsilon \approx -5$ to −30‰) or NH_4^+ ($\varepsilon \approx -30$‰), biological assimilation of NH_4^+ ($\varepsilon \approx -4$ to −27‰), and dissociation of NH_4^+ to NH_3 followed by volatilization of NH_3 gas [$\varepsilon \approx -42$‰ at 25°C; (*19*)]. These fractionations can be recorded in the rock record if organisms that consume the products or residual reactants get buried in sediments. For example, in modern marine sediments, the average bulk nitrogen isotopic composition is +5‰ (*31*), which results from partial denitrification in suboxic waters, followed by assimilation of the residual isotopically enriched nitrate into biomass, which transfers this signature to sedimentary archives during burial.

The isotopic effect of nitrification, which occurs when some biomass is remineralized under oxic conditions, is rarely expressed because nitrification rapidly goes to completion at even micromolar levels of dissolved oxygen (*32*). Only seasonal occurrences of partial nitrification have been reported from the Bering Sea and Lake Kinneret (*33*, *34*). It is important to note that this process generates two pools of isotopically distinct bioavailable nitrogen (nitrate and ammonium) and therefore can result in large isotopic heterogeneity. Similarly, partial assimilation of NH_4^+ creates isotopically light biomass and a residual pool of enriched NH_4^+, which may be assimilated elsewhere in the same basin. If partial assimilation of NH_4^+ dominates sedimentary nitrogen isotopes, one would expect a range from very negative to very positive values. In contrast, volatilization of

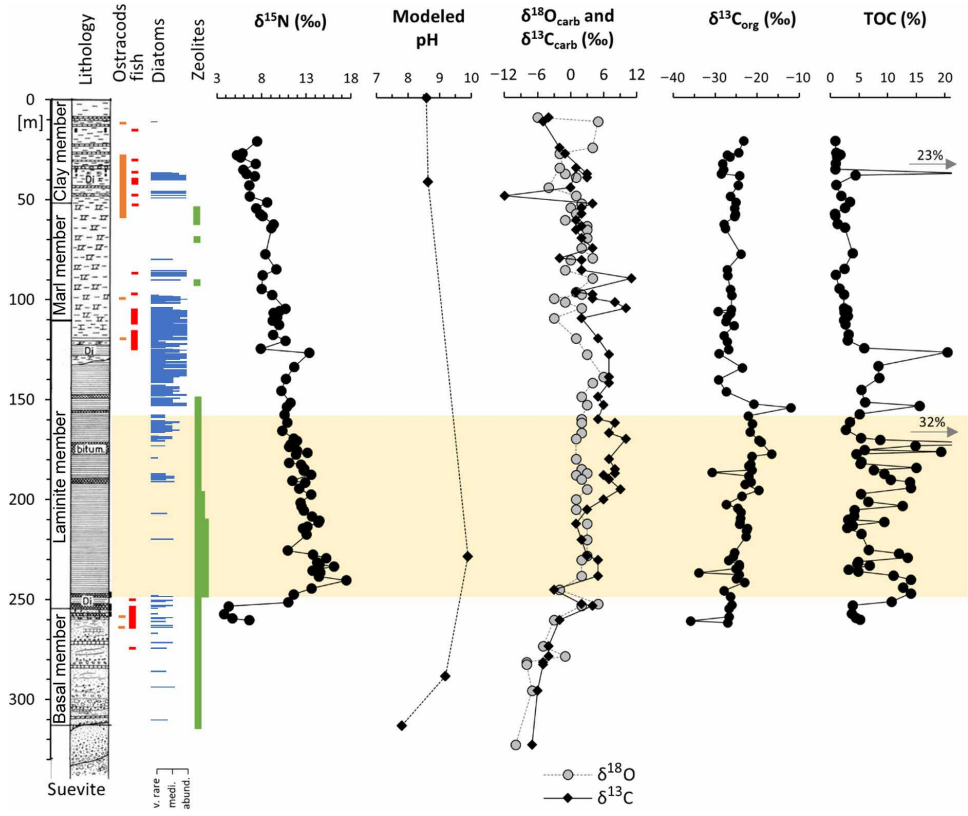

Fig. 2. Stratigraphic trends in the Nördlingen 1973 drill core. Orange shading indicates inferred hyperalkaline interval with coinciding high modeled pH and high $\delta^{15}N$, $\delta^{18}O_{carb}$, $\delta^{13}C_{carb}$, and TOC, scarcity of macrofauna, and abundant diagenetic zeolite minerals. Lithostratigraphy is taken from Füchtbauer *et al.* (*10*), $\delta^{18}O_{carb}$ and $\delta^{13}C_{carb}$ are taken from Rothe and Hoefs (*12*), and the pH model is taken from Arp *et al.* (*8*). Diatom abundances are according to Schauderna (*45*).

NH_3 gas leaves behind a uniform, isotopically enriched pool of dissolved fixed nitrogen—similar to partial denitrification. The relatively high and fairly uniform $\delta^{15}N$ values of up to +17‰ in the Ries crater are therefore most plausibly explained by either denitrification or NH_3 volatilization, but the two mechanisms cannot be unambiguously distinguished from each other via $\delta^{15}N$ data alone.

The vast majority of Holocene lakes display $\delta^{15}N$ values in the range of +1 to +4‰ (*35*), which is likely a reflection of widespread biological N_2 fixation in terrestrial and lacustrine environments with only minor secondary processing of fixed nitrogen. Significantly higher values up to +18‰ have, to our knowledge, only been reported from evaporitic modern lakes (*21*, *36*). One possible explanation for those high values is partial loss of NH_3 under high-pH conditions. This mechanism requires an oxygen-deficient environment such that diagenetically produced NH_4^+ is not quantitatively oxidized before conversion to NH_3 and escape into the atmosphere. However, redox stratification also leaves open the possibility that the high $\delta^{15}N$ values from these environments are caused by denitrification rather than NH_3 escape.

In the case of the Ries crater sediments, $\delta^{15}N$ covaries with pH values modeled by Arp *et al.* (Fig. 2) (*8*), who used modern groundwaters to infer the composition of fluids in equilibrium with Ries-related impact facies. $\delta^{15}N$ also covaries with abundances of analcime and clinoptilolite, which form during alteration of glass—a process that is known to result in high alkalinity and high pH in experimental and natural settings (*15*) (although the presence of these minerals alone is not diagnostic of a particular pH range). When the alkaline fluids generated by this water-glass interaction undergo evaporation, pH increases further because protons are consumed by reaction with HCO_3^- (*14*). To further test the plausibility of these processes, we constructed a model in Geochemist's Workbench (see Materials and Methods) where we first let suevite glass react with water and then allowed the resulting fluid to evaporate (Fig. 4, A and B). With the dissolution of only 0.4 g/liter of suevite glass [composition taken from (*37*)], the calculated pH of pure water buffered by atmospheric CO_2 increases to 8.3 (Fig. 4A). Subsequent evaporation raises the pH of this fluid to 9.3 (Fig. 4B). If the fluid is separated from the atmospheric CO_2 reservoir before reacting with the glass, as would be the case in the subsurface, the dissolution of 0.4 g/liter of glass would yield a pH of 10.2 (Fig. 4A). These values are consistent with previous models based on modern groundwaters (*8*) and are high enough for the conversion of a significant fraction of NH_4^+ to NH_3 (Fig. 4C), followed by NH_3 volatilization and isotopic enrichment (Fig. 4D). The high $\delta^{15}N$ values in the lower bituminous laminite interval of the Ries crater (256- to 200-m core depth) are therefore consistent with the effects of high pH, enriching the information gained from the presence of clays, carbonates, and zeolite minerals alone.

Arp *et al.* (*8*) argued that the lake became progressively more saline over time (i.e., stratigraphically upward in the core), but pH dropped when the major source rock of solutes switched from suevite and crystalline rocks to Bunte Breccia and Jurassic carbonate. A progressive increase in salinity and thus stagnation of the water column is supported by $\delta^{18}O_{carb}$ (Fig. 2) (*12*) and $\delta^{13}C_{org}$ (Fig. 2), which peak in the upper third of the bituminous laminite member

Table 1. Geochemical data from core Nördlingen 1973. Average reproducibility for $\delta^{15}N$ and $\delta^{13}C_{org}$ are 0.4‰ (1 SD) and 0.1‰, respectively. Average relative errors (1 SD/mean) are 6.5% for TN and 4.4% for TOC. Notes highlight enrichment in organic carbon. n.d., not determined.

Depth (m)	Notes	$\delta^{15}N$ (‰)	$\delta^{13}C_{org}$ (‰)	TN (wt %)	TOC (wt %)
Claystone member (centimeter-scale laminated mud, dark gray)					
21.55		7.47	−23.23	0.04	0.88
27.55		5.86	−24.41	0.07	1.01
28.55		5.21	−27.23	0.10	1.68
29.55		5.65	−26.49	0.07	1.13
32.95		7.31	−28.25	0.09	0.95
35.95		5.92	−28.03	0.09	0.87
37.95	Coal seam	6.31	−28.61	0.59	23.46
38.95		7.23	−24.18	0.17	4.37
43.58		6.62	−24.61	0.08	0.99
49.1		6.64	−26.37	0.12	1.87
Marl member (calcareous pale gray mudstone, massive to centimeter-scale bedding)					
52.1		8.63	−25.09	0.16	3.36
55.1		7.39	−25.45	0.14	2.56
58.1		7.84	−25.18	0.08	0.77
59.1		8.09	−25.42	0.06	0.82
63.1		9.35	−27.96	0.12	1.21
65.1		9.10	−27.62	0.16	2.51
78		8.43	−23.88	0.24	3.87
85.7		9.63	−27.14	0.14	2.43
88.7		8.11	−27.10	0.11	0.95
95.5		7.99	−26.41	0.10	1.54
98.5		9.20	−26.10	0.12	2.32
105.5		10.65	−26.17	0.16	2.39
106.5		10.02	−29.33	0.17	2.96
107.5		9.35	−26.38	0.16	2.46
109.5		9.75	−27.18	0.16	3.02
Laminite member (millimeter-scale plane laminated mudstone, carbonaceous to bituminous)					
111.5		9.24	−27.46	0.17	2.32
113.5		9.96	−25.57	0.13	2.59
118.5		9.29	−27.96	0.14	3.14
121.5		10.68	−27.14	0.14	3.00
125.5		7.91	−26.81	0.22	5.88
127.5	Bituminous	13.33	−29.19	0.48	20.44
134.5		11.65	−23.53	0.36	8.32
140.5		10.70	−29.29	0.34	8.50
146.5		10.20	−27.42	0.24	5.42
152.5		11.23	−20.86	0.29	6.00
154.5	Bituminous	10.80	−11.96	0.44	15.56
158.5		10.57	−22.12	0.23	5.05
162.5		10.85	−21.14	0.21	3.43
166.5		10.31	−21.70	0.18	2.70
170.5		11.58	−19.64	0.25	5.33

continued on next page

Depth (m)	Notes	$\delta^{15}N$ (‰)	$\delta^{13}C_{org}$ (‰)	TN (wt %)	TOC (wt %)
171.5		11.95	−19.10	0.38	8.65
173.5	Bituminous	11.25	nd	0.31	31.82
174.5	Bituminous	11.08	nd	0.28	14.84
176.5		11.94	nd	0.26	5.96
177.5	Bituminous	13.12	−16.62	0.44	19.30
178.5		11.86	−21.23	0.24	4.51
182.5		11.10	−21.62	0.30	5.37
183.5		12.42	−22.07	0.27	5.21
185.5	Bituminous	12.78	−21.26	0.55	14.96
186.5	Bituminous	12.72	−30.84	0.37	7.57
188.5	Bituminous	13.52	−21.99	0.43	9.39
191.5	Bituminous	11.42	−21.48	0.53	10.50
192.5	Bituminous	12.85	−22.90	0.43	13.90
195.5	Bituminous	12.20	−19.65	0.38	13.98
198.5		13.53	−23.66	0.41	5.28
202.5		12.34	−27.38	0.65	6.62
204.5	Bituminous	12.46	−24.65	0.78	12.58
206.5		12.73	−23.91	0.32	4.21
209.5		13.66	−24.03	0.30	4.14
211.5		14.48	−24.16	0.22	3.05
212.5		14.38	−24.20	0.58	9.36
214.5		13.13	−22.35	0.33	3.84
215.5		12.63	−22.57	0.30	2.95
218.5		13.05	−22.72	0.49	5.39
226.5		10.91	−25.47	0.82	6.64
228.5	Bituminous	13.73	−25.76	0.61	11.98
230.5	Bituminous	15.24	−26.84	0.61	13.50
232.5		14.19	−24.36	0.33	4.85
233.5		14.46	−24.32	0.34	4.71
234.5		16.09	−25.09	0.35	6.87
236.5		13.67	−34.00	0.30	3.14
237.5		14.56	−24.31	0.25	4.85
239.5	Bituminous	14.39	−24.94	0.44	11.00
241.5	Bituminous	17.47	−23.03	0.59	13.98
245.5	Bituminous	13.60	−27.99	0.43	12.66
248.5	Bituminous	11.60	−26.44	0.43	13.99
252.5	Bituminous	10.95	−26.09	0.19	10.68
254.5		4.29	−26.73	0.12	3.85
Basal member (sandstone with interlaminated carbonaceous mudstone)					
258.5		3.82	−26.71	0.11	3.72
260.5		4.73	−35.97	0.13	4.45
261.5		6.64	−27.03	0.10	5.20

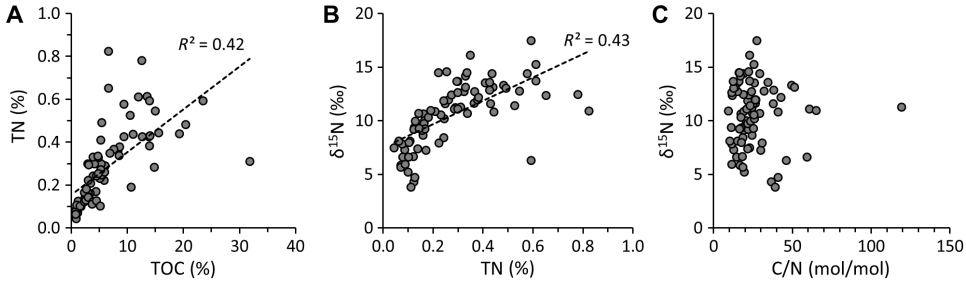

Fig. 3. Carbon-nitrogen scatterplots. (**A**) Covariance between TOC and TN. (**B**) Covariance between TN δ^{15}N. (**C**) Lack of covariance between molar organic carbon to TN ratios and δ^{15}N indicating absence of metamorphic alteration.

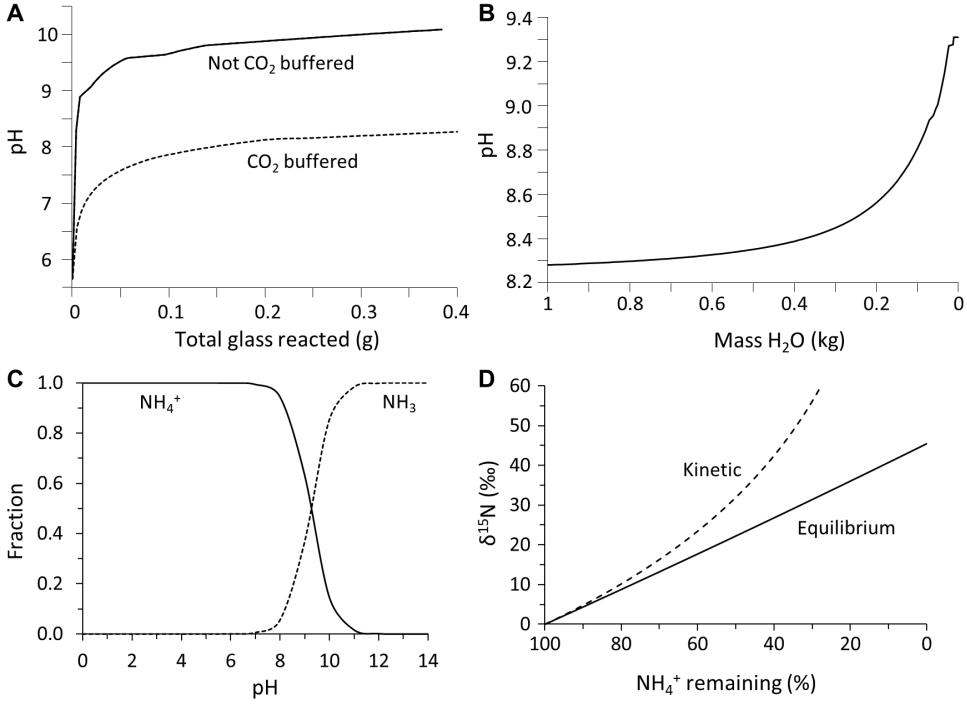

Fig. 4. Model calculations and nitrogen behavior. (**A**) Model calculation of glass dissolution in nearly pure water with either fixed atmospheric P_{CO_2} (buffered) or progressively consumed CO_2 (not buffered). The latter simulates a water-glass reaction in the subsurface (see Materials and Methods for details on input parameters). (**B**) Model calculation of evaporation of fluid after reaction with 0.4 g of glass from (A) and in constant equilibrium with atmospheric CO_2. Both scenarios of (A) result in the same evaporation effect because the load of dissolved solids is the same. (**C**) pH relationship of ammonium (NH_4^+) and ammonia (NH_3) at standard pressure and temperature. (**D**) Isotopic effect of NH_3 volatilization on residual dissolved NH_4^+ for kinetic and equilibrium fractionation models.

(170- to 140-m core depth) and stay relatively elevated in the overlying marl member, consistent with high levels of evaporation during this interval (*8*). Biomarker records further indicate anoxic bottom waters for major parts of the depositional history of the lake (*8*). The decline of δ^{15}N up-section despite a likely persistence of oxygen deficiency, starting from its peak at the base of the bituminous laminite member (256-m core depth), indicates that redox stratification was not the dominant cause of the strong isotopic enrichments in nitrogen isotopes lower in the core. Denitrification alone can therefore not explain these data. Instead, high-pH conditions as inferred from the lower part of the core (256- to 200-m core depth) appear to have been necessary to generate δ^{15}N values significantly above +10‰. Our data thus provide strong evidence that δ^{15}N can serve as a pH indicator in paleolacustrine environments. The basic physicochemical nature of this proxy makes it readily extendable to Mars and high-pH bodies such as Enceladus and exoplanetary water worlds.

CONCLUSION

The nitrogen isotope record of the Miocene Ries crater lake shows unusually high δ^{15}N values up to +17‰ during an interval with independent mineralogical and paleontological evidence of high pH and redox stratification (*8*). δ^{15}N values decreased when the water chemistry of the lake transitioned to circumneutral pH, despite a persistence of evidence for low-oxygen conditions in lake bottom waters (monimolimnion). This combination of observations indicates that redox stratification was insufficient to generate δ^{15}N values above +10‰. Instead, high pH appears to have been required, suggesting that NH_3 volatilization played a significant role in elevating

$\delta^{15}N$. Our data are thus strong evidence that nitrogen isotopes can serve as a paleo-pH indicator around a threshold of ~9.2—i.e., the pK_a of the NH_4^+/NH_3 transformation. This proxy should be a valuable addition to future Mars exploration because high-pH alkaline environments host the most bioproductive natural ecosystems on Earth (*4*), including the highest diversity of cyanobacteria (*38*). The more mafic composition of the Martian crust compared to the crystalline basement (gneiss, granite, amphibolite) under the Ries crater should only serve to enhance the utility of this proxy, since weathering of mafic glass has a relatively stronger effect on raising the pH than felsic glass (*15*). Furthermore, numerous prebiotic reactions may have been facilitated in high-pH settings, including the formation of carbohydrates, the polymerization of hydrogen cyanide into amino acids, and the phosphorylation of nucleotides (*39*–*41*). Reduced, non-ammonium nitrogenous compounds (e.g., pyridine) have recently been observed within indigenous organic material of the Tissint meteorite (*42*). Such compounds may be indicative of electrochemical reduction of N_2 to NH_4^+ (*42*). These observations indicate that the nitrogen isotope ratios have the potential to serve as a powerful proxy for high pH on the Martian surface. $\delta^{15}N$ signals indicative of ammonia volatilization would allow distinguishing between high alkalinity and high pH. Such a distinction would have implications for atmospheric composition because the co-occurrence of high total alkalinity based on mineralogical observations and circumneutral pH, under which ammonia volatilization is suppressed, would point toward relatively elevated P_{CO_2} (partial pressure of CO_2) of at least 0.5 bar (*43*). In contrast, a high pH, as suggested by high $\delta^{15}N$ values, would place an upper limit on P_{CO_2}. An independent pH constraint would thus help address the long-standing problem of persistent liquid water despite a faint young Sun by helping constrain the amount of CO_2 in the ancient Martian atmosphere. $\delta^{15}N$ measurements in Martian sedimentary strata may be an important analytical tool in the upcoming era of sample return, helping to identify high-pH paleoenvironments with a high potential for habitability and an independent origin of life.

MATERIALS AND METHODS

The outer rims of the core samples were trimmed with a manually operated rock chipper, and the interiors were hammered into subcentimeter-sized chips and dehydrated at 50°C for a minimum of 48 hours. The rock chips were then pulverized in a ball mill and stored in scintillation vials. For isotopic analyses, roughly 0.5 g of powder was decarbonated with 2 N HCl at 60°C overnight and washed three times with 18 megohm cm^{-1} deionized H_2O (*20*). The dried residues were weighed into tin capsules and analyzed for organic carbon and TN isotopes at the University of St. Andrews, using an EA IsoLink coupled to a MAT 253 isotope ratio mass spectrometer via a ConFlo IV. The data were calibrated with international reference materials USGS-40 and USGS-41. Long-term reproducibility was tracked with the rock standard SGR-1 (untreated), for which we obtained a $\delta^{15}N$ value of 17.4 ± 0.5‰—in good agreement with previous studies (*44*). Data are expressed in standard delta notation relative to Vienna Pee Dee belemnite for $\delta^{13}C_{org}$ and relative to air for $\delta^{15}N$. To verify that acidification had no adverse effects on our isotopic data, a subset of samples was treated with 2 N HCl a second time. The obtained results were within analytical precision of the first set of measurements with single acid treatments.

To test the plausibility of our interpretation, a geochemical model was constructed using the React module in Geochemist's Workbench. One kilogram of H_2O in equilibrium with CO_2 gas (3.5×10^{-4} bar) and O_2 gas (0.2 bar) in the Basis pane was reacted with suevite glass (*37*), simulated by SiO_2 (63.3 mg), Al_2O_3 (14.7 mg), FeO (5.2 mg), MgO (3 mg), CaO (4.3 mg), Na_2O (2.7 mg), and K_2O (2.8 mg) in the Reactants pane. Elements were entered as oxides to simulate the amorphous nature of glass. For the model to run, the Basis needed to contain traces of each element, which were chosen as $SiO_{2(aq)}$ (0.1 nM), Al^{3+} (0.1 nM), Fe^{2+} (0.001 nM), Mg^{2+} (1 nM), Ca^{2+} (1 nM), Na^+ (1 nM), K^+ (1 nM), Cl^- (1 nM), and SO_4^{2-} (1 nM). pH was used as a charge balance. These concentrations are so low that this is essentially pure water; changes in these concentrations by a factor of 10 had no effect on the outcome of the model. For models of a system that is buffered by the atmosphere, the fugacities of CO_2 and O_2 were fixed in the Reactants pane. Once the solution had equilibrated with the glass, the end composition of the new solution was transferred into the Basis. A new simulation was run where H_2O was progressively removed in the Reactants pane, simulating evaporation. Again, the fugacities of CO_2 and O_2 were fixed to simulate an atmosphere-buffered system. Results were plotted in Gtplot.

REFERENCES AND NOTES

1. B. L. Ehlmann, J. F. Mustard, C. I. Fassett, S. C. Schon, J. W. Head III, D. J. Des Marais, J. A. Grant, S. L. Murchie, Clay minerals in delta deposits and organic preservation potential on Mars. *Nat. Geosci.* **1**, 355–358 (2008).
2. T. A. Goudge, J. F. Mustard, J. W. Head, C. I. Fassett, S. M. Wiseman, Assessing the mineralogy of the watershed and fan deposits of the Jezero crater paleolake system, Mars. *J. Geophys. Res.* **120**, 775–808 (2015).
3. V. Chevrier, F. Poulet, J.-P. Bibring, Early geochemical environment of Mars as determined from thermodynamics of phyllosilicates. *Nature* **448**, 60–63 (2007).
4. W. D. Grant, B. E. Jones, Alkaline environments, in *Encyclopedia of Microbiology* (Academic Press, ed. 2, 2000), vol. 1, pp. 126–133.
5. G. R. Osinski, L. L. Tornabene, N. R. Banerjee, C. S. Cockell, R. Flemming, M. R. M. Izawa, J. McCutcheon, J. Parnell, L. J. Preston, A. E. Pickersgill, A. Pontefract, H. M. Sapers, G. Southam, Impact-generated hydrothermal systems on Earth and Mars. *Icarus* **224**, 347–363 (2013).
6. T. Kenkmann, F. Schönian, Ries and Chicxulub: Impact craters on Earth provide insights for Martian ejecta blankets. *Meteorit. Planet. Sci.* **41**, 1587–1603 (2006).
7. S. Sturm, G. Wulf, D. Jung, T. Kenkmann, The Ries impact, a double-layer rampart crater on Earth. *Geology* **41**, 531–534 (2013).
8. G. Arp, M. Blumenberg, B. T. Hansen, D. Jung, C. Kolepka, O. Lenz, N. Nolte, K. Poschlod, A. Reimer, V. Thiel, Chemical and ecological evolution of the Miocene Ries impact crater lake, Germany: A reinterpretation based on the Enkingen (SUBO 18) drill core. *Geol. Soc. Am. Bull.* **125**, 1125–1145 (2013).
9. J. Pohl, D. Stoeffler, H. V. Gall, K. Ernstson, in *Impact and Explosion Cratering: Planetary and Terrestrial Implications*, D. J. Roddy, R. O. Pepin, R. B. Merrill, Eds. (Pergamon Press, 1977), pp. 343–404.
10. H. Füchtbauer, G. von der Brelie, R. Dehm, U. Förstner, H. Gall, R. Höfling, J. Hoefs, A. Hollerback, H. Hufnagel, B. Jankowsky, W. Jung, H. Malz, H. Mertes, P. Rothe, M. Salger, H. Wehner, M. Worf, Tertiary lake sediments of the Ries, research borehole Nördlingen 1973—A summary. *Geologica Bavarica* **75**, 13–19 (1977).
11. G. Arp, S. Schultz, V. Karius, J. W. Head III, Ries impact crater sedimentary conglomerates: Sedimentary particle 'impact pre-processing', transport distances and provenance, and implications for Gale crater conglomerates, Mars. *Icarus* **321**, 531–598 (2019).
12. P. Rothe, J. Hoefs, Isotopen-geochemische Untersuchungen an Karbonaten der Ries-See-Sedimente der Forschungbohrung Nördlingen 1973. *Geologica Bavarica* **75**, 59–66 (1977).
13. S. W. Ruff, Spectral evidence for zeolite in the dust on Mars. *Icarus* **168**, 131–143 (2004).
14. R. M. Garrels, F. T. Mackenzie, in *Equilibrium Concepts in Natural Water Systems*, W. Stumm, Ed. (American Chemical Society, 1967), chap. 10, pp. 222–242.
15. S. R. Gislason, H. P. Eugster, Meteoric water-basalt interaction. I: A laboratory study. *Geochim. Cosmochim. Acta* **51**, 2827–2840 (1987).
16. V. Sautter, M. J. Toplis, R. C. Wiens, A. Cousin, C. Fabre, O. Gasnault, S. Maurice, O. Forni, J. Lasue, A. Ollila, J. C. Bridges, N. Mangold, S. Le Mouélic, M. Fisk, P.-Y. Meslin, P. Beck, P. Pinet, L. Le Deit, W. Rapin, E. M. Stolper, H. Newsom, D. Dyar, N. Lanza, D. Vaniman, S. Clegg, J. J. Wray, In situ evidence for continental crust on early Mars. *Nat. Geosci.* **8**, 605–609 (2015).

17. J. P. Grotzinger, D. Y. Sumner, L. C. Kah, K. Stack, S. Gupta, L. Edgar, D. Rubin, K. Lewis, J. Schieber, N. Mangold, R. Milliken, P. G. Conrad, D. Des Marais, J. Farmer, K. Siebach, F. Calef III, J. Hurowitz, S. M. McLennan, D. Ming, D. Vaniman, J. Crisp, A. Vasavada, K. S. Edgett, M. Malin, D. Blake, R. Gellert, P. Mahaffy, R. C. Wiens, S. Maurice, J. A. Grant, S. Wilson, R. C. Anderson, L. Beegle, R. Arvidson, B. Hallet, R. S. Sletten, M. Rice, J. Bell III, J. Griffes, B. Ehlmann, R. B. Anderson, T. F. Bristow, W. E. Dietrich, G. Dromart, J. Eigenbrode, A. Fraeman, C. Hardgrove, K. Herkenhoff, L. Jandura, G. Kocurek, S. Lee, L. A. Leshin, R. Leveille, D. Limonadi, J. Maki, S. McCloskey, M. Meyer, M. Minitti, H. Newsom, D. Oehler, A. Okon, M. Palucis, T. Parker, S. Rowland, M. Schmidt, S. Squyres, A. Steele, E. Stolper, R. Summons, A. Treiman, R. Williams, A. Yingst; MSL Science Team, A habitable fluvio-lacustrine environment at Yellowknife Bay, Gale Crater, Mars. *Science* **343**, 1242777 (2014).
18. R. Jellison, L. G. Miller, J. M. Melack, G. L. Dana, Meromixis in hypersaline Mono Lake, California. II: Nitrogen fluxes. *Limnol. Oceanogr.* **38**, 1020–1039 (1993).
19. L. Li, B. Sherwood Lollar, H. Li, U. G. Wortmann, G. Lacrampe-Couloume, Ammonium stability and nitrogen isotope fractionations for NH_4^+-$NH_{3(aq)}$-$NH_{3(gas)}$ systems at 20-70°C and pH of 2-13: Applications to habitability and nitrogen cycling in low-temperature hydrothermal systems. *Geochim. Cosmochim. Acta* **84**, 280–296 (2012).
20. E. E. Stüeken, R. Buick, A. J. Schauer, Nitrogen isotope evidence for alkaline lakes on late Archean continents. *Earth Planet. Sci. Lett.* **411**, 1–10 (2015).
21. M. R. Talbot, T. Johannessen, A high resolution palaeoclimatic record for the last 27,500 years in tropical west Africa from the carbon and nitroen isotopic composition of lacustrine organic matter. *Earth Planet. Sci. Lett.* **110**, 23–37 (1992).
22. J. W. Collister, J. M. Hayes, in *Geochemical, Biogeochemical, and Sedimentological Studies of the Green River Formation, Wyoming, Utah, and Colorado*, M. L. Tuttle, Ed. (U.S. Geological Survey, 1973).
23. P. Menzel, B. Gaye, M. G. Wiesner, S. Prasad, M. Stebich, B. K. Das, A. Anoop, N. Riedel, N. Basavaiah, Influence of bottom water anoxia on nitroen isotopic ratios and amino acid contributions of recent sediments from small eutrophic Lonar Lake, central India. *Limnol. Oceanogr.* **58**, 1061–1074 (2013).
24. G. Arp, B. T. Hansen, A. Pack, A. Reimer, B. C. Schmidt, K. Simon, D. Jung, The soda lake-mesosaline halite lake transition in the Ries impact crater basin (drilling Löpsingen 2012, Miocene, southern Germany). *Facies* **63**, 1 (2017).
25. P. J. Müller, CN ratios in Pacific deep-sea sediments: Effect of inorganic ammonium and organic nitrogen compounds sorbed by clays. *Geochim. Cosmochim. Acta* **41**, 765–776 (1977).
26. R. S. Robinson, M. Kienast, A. L. Albuquerque, M. Altabet, S. Contreras, R. De Pol Holz, N. Dubois, R. Francois, E. Galbraith, T.-C. Hsu, T. Ivanochko, S. Jaccard, S.-J. Kao, T. Kiefer, S. Kienast, M. Lehmann, P. Martinez, M. McCarthy, J. Möbius, T. Pedersen, T. M. Quan, E. Ryabenko, A. Schmittner, R. Schneider, A. Schneider-Mor, M. Shigemitsu, D. Sinclair, C. Somes, A. Studer, R. Thunell, J.-Y. Yang, A review of nitrogen isotopic alteration in marine sediments. *Paleoceanography* **27**, PA4203 (2012).
27. E. E. Stüeken, J. Zaloumis, J. Meixnerová, R. Buick, Differential metamorphic effects on nitrogen isotopes in kerogen extracts and bulk rocks. *Geochim. Cosmochim. Acta* **217**, 80–94 (2017).
28. M. Wolf, Kohlenpetrographische Untersuchungen der See-Sedimente der Forschungsbohrung Nördlingen 1973 und Vergleich mit anderen Untersuchungsergebnissen aus dem Ries. *Geologica Bavarica* **75**, 127–138 (1977).
29. T. W. Horton, W. F. Defliese, A. K. Tripati, C. Oze, Evaporation induced ^{18}O and ^{13}C enrichment in lake systems: A global perspective on hydrologic balance effects. *Quat. Sci. Rev.* **131**, 365–379 (2016).
30. E. E. Stüeken, M. A. Kipp, M. C. Koehler, R. Buick, The evolution of Earth's biogeochemical nitrogen cycle. *Earth Sci. Rev.* **160**, 220–239 (2016).
31. J.-E. Tesdal, E. D. Galbraith, M. Kienast, Nitrogen isotopes in bulk marine sediment: Linking seafloor observations with subseafloor records. *Biogeosciences* **10**, 101–118 (2013).
32. F. Lipschultz, S. C. Wofsy, B. B. Ward, L. A. Codispoti, G. Friedrich, J. W. Elkins, Bacterial transformations of inorganic nitrogen in the oxygen-deficient waters of the Eastern Tropical South Pacific Ocean. *Deep Sea Res. Part A* **37**, 1513–1541 (1990).
33. L. V. Morales, J. Granger, B. X. Chang, M. G. Prokopenko, B. Plessen, R. Gradinger, D. M. Sigman, Elevated $^{15}N/^{14}N$ in particulate organic matter, zooplankton, and diatom frustule-bound nitrogen in the ice-covered water column of the Bering Sea eastern shelf. *Deep Sea Res. Part II* **109**, 100–111 (2014).
34. O. Hadas, M. A. Altabet, R. Agnihotri, Seasonally varying nitrogen isotope biogeochemistry of particulate organic matter (POM) in Lake Kinneret, Israel. *Limnol. Oceanogr.* **54**, 75–85 (2009).
35. K. K. McLauchlan, J. J. Williams, J. M. Craine, E. S. Jeffers, Changes in global nitrogen cycling during the Holocene epoch. *Nature* **495**, 352–355 (2013).
36. D. L. Newell, J. L. Jensen, C. M. Frantz, M. D. Vanden Berg, Great Salt Lake (Utah) microbialite $\delta^{13}C$, $\delta^{18}O$, and $\delta^{15}N$ record fluctuations in lake biogeochemistry since the Late Pleistocene. *Geochem. Geophys. Geosyst.* **18**, 3631–3645 (2017).
37. T. W. Vennemann, A. Morlok, W. von Engelhardt, K. Kyser, Stable isotope composition of impact glasses from the Nördlinger Ries impact crater, Germany. *Geochim. Cosmochim. Acta* **65**, 1325–1336 (2001).
38. G. A. Zavarzin, Epicontinental soda lakes as probable relict biotopes of terrestrial biota formation. *Microbiology* **62**, 473–479 (1993).
39. H.-J. Kim, A. Ricardo, H. I. Illangkoon, M. J. Kim, M. A. Carrigan, F. Frye, S. A. Benner, Synthesis of carbohydrates in mineral-guided prebiotic cycles. *J. Am. Chem. Soc.* **133**, 9457–9468 (2011).
40. J. P. Ferris, W. J. Hagan Jr., HCN and chemical evolution: The possible role of cyano compounds in prebiotic synthesis. *Tetrahedron* **40**, 1093–1120 (1984).
41. S. Kempe, J. Kazmierczak, Biogenesis and early life on Earth and Europa: Favored by an alkaline ocean? *Astrobiology* **2**, 123–130 (2002).
42. A. Steele, L. G. Benning, R. Wirth, S. Siljeström, M. D. Fries, E. Hauri, P. G. Conrad, K. Rogers, J. Eigenbrode, A. Schreiber, A. Needham, J. H. Wang, F. M. McCubbin, D. Kilcoyne, J. D. Rodriguez-Blanco, Organic synthesis on Mars by electrochemical reduction of CO_2. *Sci. Adv.* **4**, eaat5118 (2018).
43. R. Wordsworth, Y. Kalugina, S. Lokshtanov, A. Vigasin, B. Ehlmann, J. Head, C. Sanders, H. Wang, Transient reducing greenhouse warming on early Mars. *Geophys. Res. Lett.* **44**, 665–671 (2017).
44. K. O. Dennen, C. A. Johnson, M. L. Otter, S. R. Silva, G. A. Wandless, $\delta^{15}N$ and non-carbonate $\delta^{13}C$ values for two petroleum source rock reference materials and a marine sediment reference material, U.S. Geological Survey Open-File Report 2006–1071, (2006); https://doi.org/10.3133/ofr20061071.
45. H. Schauderna, Die Diatomeenflora aus den miozänen Seeablagerungen im Nördlinger Ries. *Palaeontographica* **188**, 83–193 (1983).

Acknowledgments

Funding: This research was financially supported by the Leverhulme Trust to T.W.L. E.E.S. acknowledges start-up funds from the University of St. Andrews. The NASA Astrobiology Institute under Cooperative Agreement no. NNA15BB03A issued through the Science Mission Directorate also provided funds as did a NASA Fellowship in support of C.T. under Cooperative Agreement no. 80NSSC19K1739 issued through the NASA Office of STEM Engagement. E.E.S. thanks Meinolf and Karin Koch for their hospitality during the field work. Two anomymous reviewers are thanked for constructive comments that improved the manuscript. **Author contributions:** E.E.S. and T.W.L. developed the project. E.E.S., C.T., T.W.L., G.A., and D.J. collected the samples. C.T. carried out the sample preparation and analyses with support from E.E.S. E.E.S. constructed the geochemical model and wrote the manuscript with contributions from all authors. **Competing interests:** The authors declare that they have no competing interests. **Data and materials availability:** All data reported in this manuscript are included in Table 1. All data needed to evaluate the conclusions in the paper are present in the paper. Additional data related to this paper may be requested from the authors.

Submitted 10 June 2019
Accepted 9 December 2019
Published 26 February 2020
10.1126/sciadv.aay3440

Citation: E. E. Stüeken, C. Tino, G. Arp, D. Jung, T. W. Lyons, Nitrogen isotope ratios trace high-pH conditions in a terrestrial Mars analog site. *Sci. Adv.* **6**, eaay3440 (2020).

Nitrogen isotope ratios trace high-pH conditions in a terrestrial Mars analog site

Eva E. Stüeken, Christopher Tino, Gernot Arp, Dietmar Jung and Timothy W. Lyons

Sci Adv **6** (9), eaay3440.
DOI: 10.1126/sciadv.aay3440